IOP Conf. Series: Materials Science and Engineering **232** (2017) 012055 doi:10.1088/1757-899X/232/1/012055

Thermal modelling of a dry revolving vane compressor

K T Ooi [1,3] and **K T Aw**[2,4]

[1,2] School of Mechanical and Aerospace Engineering, Nanyang Technological University, 50 Nanyang Avenue, Singapore 639798

[3] mktooi@ntu.edu.sg
[4] ktaw1@e.ntu.edu.sg

Abstract. The lubricant used in compressors serves to lubricate, to seal the gaps to reduce internal leakage and to a certain extent, to cool. However, a lubricant free compressor is attractive if lubricants become a source of contaminant, or in areas where the compressor needs be placed under any orientation, such as those in military or portable computing.

In this paper, a thermal model for a dry revolving vane compressor is presented. This thermal model sets out to predict the steady-state operating temperatures of the compressor components. The lumped thermal conductance method was employed. The results of the components temperature will be presented and discussed. A high potential for overheating is observed at the shaft bearings.

1. Introduction

In a lubricant free compressor, dry sliding friction between the moving components would generate excessive heat in the compressor which may compromise the reliability of the compressor.

The lumped thermal conductance method was employed for thermal modelling of various compressors [1–3] including the rolling piston compressor [4]. As the RV compressor shares many similarities with that of the rolling piston, this same method would be used for modelling the heat transfer between the components in the compressor prototype.

2. Assumptions and sub-division of components

The six major components in the compressor are subdivided into 14 elements with simple geometric shapes, as shown in Figure 1. The rotor elements r2, r3 and r4 are concentric.

The following assumptions are made for the thermal model:

- Steady-state condition with isothermal elements
- Since the eccentricity is small (7.5 mm) as compared to the housing diameter (160.0 mm) all cylindrical components/holes are assumed to be concentric.
- Thermal contact resistance between steel components are negligible
- Radiation heat transfer among compressor components is negligible

Existing convection correlations at the solid-fluid interfaces [5–10] are used. Thermal contact and dry sliding friction models from literature [11, 12] will be employed for modelling heat generation and transfer at rubbing interfaces.

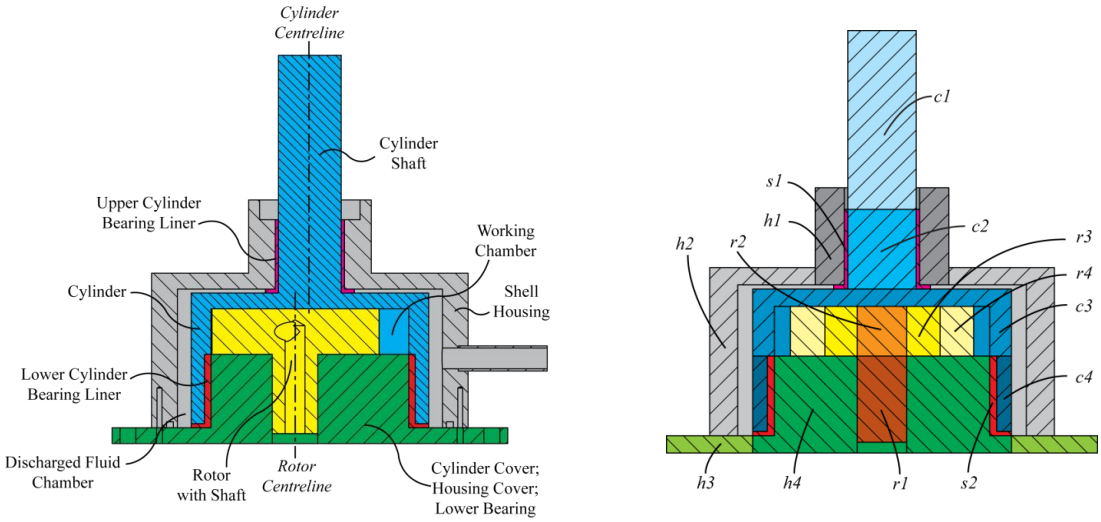

(a): Prototype Cross-section **(b): Cross-section with Simplified Geometry**

Figure 1: Subdivision of RV Components

3. Heat transfer model

3.1 Heat Transfer Equations

Applying the steady state First Law of Thermodynamics [13] to the solid element and ignoring thermal expansion, yields heat transfer equation (1).

$$\sum_i h_i A_i \Delta T_i + \dot{Q}_{gen} = \sum_o h_o A_o \Delta T_o \tag{1}$$

The one-dimensional heat transfer equations [5] are written as Equation (2) for conduction, convection and radiation respectively.

$$\dot{Q} = hA\Delta T \tag{2}$$

where, for each mode of heat transfer, h is shown in equation (3) to (5).

$$h_{cond} = \frac{k}{\Delta l} \text{ or } \frac{k}{r_1 \ln\left({}^{r_2}/_{r_1}\right)} \tag{3}$$

$$h_{conv} = \frac{k}{l}\mathrm{Nu} \tag{4}$$

$$h_{radn} = \varepsilon\sigma F_{i\to j}\left(T_i + T_j\right)\left(T_i^2 + T_j^2\right) \tag{5}$$

3.2 Thermal contact model for dry sliding interfaces

The total dry frictional heat generated between two surfaces, 1 and 2 can be obtained by equations (6) to (8) [11, 14]:

$$\dot{Q}_f = F_f v_{sl} = F_f \omega_{shaft} r_{shaft} \tag{6}$$

$$\xi = \frac{R_{sl,2}}{R_{sl,1} + R_{sl,2}} \tag{7}$$

$$\left.\begin{aligned} \dot{Q}_{f,1} &= \xi \dot{Q}_f \\ \dot{Q}_{f,2} &= (1-\xi)\dot{Q}_f \\ \dot{Q}_f &= \dot{Q}_{f,1} + \dot{Q}_{f,2} \end{aligned}\right\} \tag{8}$$

The correlation for the dimensionless sliding thermal contact resistance for two rough surfaces in dry sliding contact [14], based on the material characteristics, sliding velocity, and profile of the surface

asperities, is shown in Equation (9), while Equation (10) is the corresponding thermal contact resistance value.

The asperity profile of a typical surface from the turning process [14] shown in Figure 2, and can be modelled by assuming uniform asperities with each asperity having the same height and width, separated at a constant distance as illustrated in Figure 3.

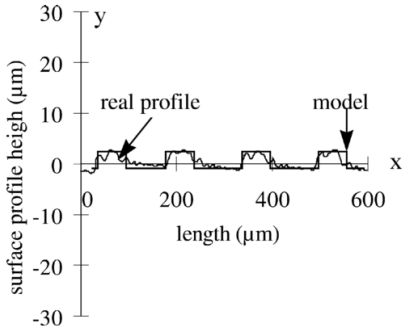

Figure 2: Aspertiy Profile of a Turned Surface [11]

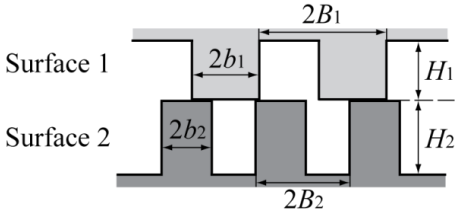

Figure 3: Assumed Asperity Profile at Interface

$$R^*_{sl,i} = 0.93\left(\frac{1}{b^*_i} - 1\right)\cdot H^*_i + 0.4\left(\frac{1}{v^*_i}\right)^{0.24}\cdot\left(\frac{1}{b^*_i} - 1\right)^{1.45}, \qquad i = 1,2 \tag{9}$$

$$R_{sl,i} = \frac{2B_i R^*_{sl,i}}{k_i} \tag{10}$$

where

$$v^*_i = \frac{2v_{sl}B_i\rho_i c_{p_i}}{k_i} \tag{11}$$

$$H^*_i = \frac{H_i}{2B_i} \tag{12}$$

$$b^*_i = \frac{b_i}{B_i} \tag{13}$$

Polyetheretherketone (PEEK) in its pure form and bearing grade PEEK are used. A comparison between the sliding thermal contact resistances of the PEEK materials and AISI 4140 steel is shown in Figure 4.

The surface properties are assumed as shown in Table 1 and the material properties are listed in Table 2.

Table 1: Asperity Properties

Property	**Value, µm**
Height, *H*	0.6
Width, 2*b*	0.5
Periodic Separation, 2*B*	1.0

Table 2: Material Properties

	Pure PEEK	**Bearing Grade PEEK**	**AISI 4140 Steel [15]**
Thermal Conductivity, W m^{-1} K^{-1}	0.27	0.82	42.7
Density, kg m^{-3}	1310	1440	7700
Specific Heat Capacity, J kg^{-1} K^{-1}	1100	1100	473

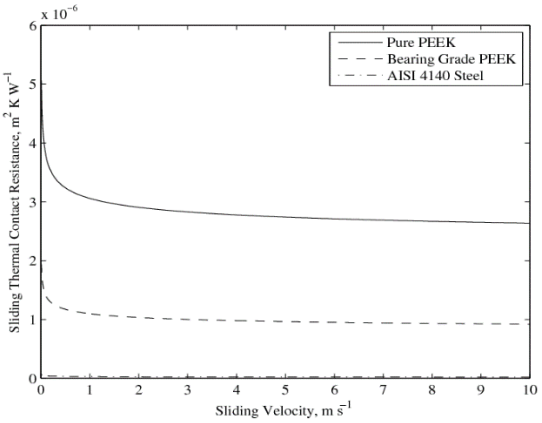

Figure 4: Comparison of Thermal Contact Resistance Between PEEK Materials & Steel

It is noted that realistic deviations from the assumed asperity dimensions would not cause the sliding thermal contact resistance of steel to have drastic changes.

From Figure 5 the heat generation coefficient for steel can be approximated to 0.99 and 0.975 when rubbing with pure PEEK and bearing grade PEEK, respectively. Hence PEEK appears to absorb negligible heat as compared to steel. Therefore, it is assumed that all friction heat is absorbed by steel. In addition, friction heat at the bearings is assumed to be split evenly between the steel shaft and bearing surfaces due to free rotation of the PEEK bearing liner.

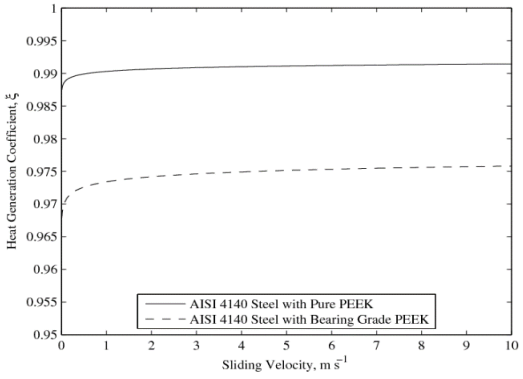

Figure 5: Heat Generation Coefficient for AISI 4140 Steel.

The steady-state temperatures of the PEEK bearing liners would be the average of the steel shaft and bearing temperatures.

3.3 Other assumptions and heat transfer correlations

The relevant heat transfer correlations for horizontal surfaces, vertical surfaces and cylindrical surfaces of the elements are presented:

i. Free convection heat transfer correlations for housing shell and base cover elements – the Nusselt number correlation for free convection [16] on the upper surface of the housing shell and lower surface of the base cover is given by Equations (14) and (15), respectively. The outer vertical surface can be treated as that of a vertical plate in which its Nusselt number [17] is given by Equation (16).

$$\mathrm{Nu} = \begin{cases} 0.54\mathrm{Ra}_{l_{ch}}^{1/4}, & 10^4 \le \mathrm{Ra}_{l_{ch}} < 10^7 \\ 0.15\mathrm{Ra}_{l_{ch}}^{1/3}, & 10^7 \le \mathrm{Ra}_{l_{ch}} < 10^{11} \end{cases} \quad (14)$$

$$\mathrm{Nu} = 0.27\mathrm{Ra}_{l_{ch}}^{1/4}, \quad 10^5 \le \mathrm{Ra}_{l_{ch}} \le 10^{10} \quad (15)$$

$$\mathrm{Nu} = \begin{cases} 0.68 + \dfrac{0.67\mathrm{Ra}_{l_{ch}}^{1/4}}{\left[1 + \left(\dfrac{0.492}{\mathrm{Pr}}\right)^{9/16}\right]^{4/9}}, & 0 < \mathrm{Ra}_{l_{ch}} \le 10^9 \\ \left[0.825 + \dfrac{0.387\mathrm{Ra}_{l_{ch}}^{1/6}}{\left(1 + \left[\dfrac{0.492}{\mathrm{Pr}}\right]^{9/16}\right)^{8/27}}\right]^2, & \mathrm{Ra}_{l_{ch}} > 10^9 \end{cases} \quad (16)$$

ii. The in-chamber convective heat transfer shown in Equation (17) by Liu and Zhou [7], was tested by Tan and Ooi [6] to be the most accurate for the RV compressor and is thus chosen.

$$\mathrm{Nu} = 0.75\overline{\mathrm{Re}}^{0.8}\overline{\mathrm{Pr}}^{0.6} \quad (17)$$

iii. Heat transfer correlations for Taylor-Couette flow are adopted for modelling the convective heat transfer in the discharge chamber between the cylinder and housing walls as shown in Equation (18) [8]. The flow in the annular gap at the endfaces is turbulent and therefore, the turbulent convective heat transfer of a flow over a flat plate can be expressed as shown in Equation (19) [5]. The speed of the flow is assumed to be the mean of the cylinder and housing wall speeds and the length would be circumferential length of the gap.

$$\mathrm{Nu} = 0.409\left(\frac{\mathrm{Ta}}{C_{geo}}\right)^{0.241}, \quad 1700 \le \left(\frac{\mathrm{Ta}}{C_{geo}}\right) \le 10^7 \quad (18)$$

$$\mathrm{Nu}_{gap} = 0.037\mathrm{Re}_{gap}^{4/5}\mathrm{Pr}^{1/3} \quad (19)$$

where

$$\mathrm{Ta} = \frac{\omega_{crit}^2\rho^2 r_{avg} r_{gap}^3}{\mu^2} \quad (20)$$

$$\omega_{crit} = \frac{\pi^4\mu^2 r_{avg}}{s r_{gap}^3 r_i^2} \quad (21)$$

$$C_{geo} = \frac{1}{s}\left(\frac{\pi^4}{1697}\right)\left(1 - \frac{r_{gap}}{2r_{avg}}\right)^{-2} \quad (22)$$

$$s = 0.0572\left(1 - \frac{0.652 r_{gap}}{r_i}\right) + 0.00056\left(1 - \frac{0.652 r_{gap}}{r_o}\right)^{-1} \quad (23)$$

$$r_{gap} = r_o - r_i \quad (24)$$

$$r_{avg} = \frac{r_o + r_i}{2} \quad (25)$$

$$\mathrm{Re}_{gap} = \frac{\rho\omega_{avg} r_{avg} l_{gap}}{\mu} \quad (26)$$

$$l_{gap} = \pi(r_o + r_i) \quad (27)$$

iv. Convective heat transfer on rotating cylinder shaft – for a high-speed rotating cylinder in quiescent air, it can be assumed that the convective heat transfer coefficient depends on only the Reynolds number [6, 7]. The correlation by Becker [9] can be used and the average Nusselt number is expressed as shown in Equation (28):

$$\mathrm{Nu} = 0.119\mathrm{Re}_r^{2/3}, \quad 800 \le \mathrm{Re}_r = \frac{2\rho\omega_{shaft} r_{shaft}^2}{\mu} \le 10^5 \quad (28)$$

v. Radiation heat transfer to surroundings – the emissivity for polished metal surfaces ranges between 0.10 and 0.40 depending on the grade of finishing. For the polished steel surface of the

housing shell, its emissivity shall be estimated to be the average of the given range (ε = 0.25). Assuming a small object radiating in an enclosure would give a view factor at unity [5], therefore, the radiation heat transfer can be expressed as shown in Equation (29) with ε = 0.25.

$$h_{radn} = 0.25\sigma(T_w + T_\infty)(T_w^2 + T_\infty^2) \tag{29}$$

3.4 Heat Transfer in the Rotor

The rotor component is made from PEEK material which has very high sliding thermal contact resistance as compared to steel. Hence, the friction heat that is absorbed by the rotor has to be dissipated in the suction line or working chambers.

3.4.1 Convective heat transfer at rotor shaft tip

One end of the rotor shaft is exposed to ambient and it can be considered as a rotating disc:

$$\mathrm{Re}_{disc} = \frac{\rho\omega_{disc}r_{disc}^2}{\mu} \tag{30}$$

As the diameter of the shaft is small (Ø23.0 mm), the rotational Reynolds number at 3000 rev min^{-1} is only 2600. Hence, the flow regime at the shaft tip is laminar. As shown by Cobb and Saunders [18] the heat transfer is best modelled by the correlation given by Wagner [19]:

$$\mathrm{Nu} = 0.335\mathrm{Re}_{disc}^{0.5}\ , \qquad \mathrm{Re}_{disc} < 2.4 \times 10^5 \tag{31}$$

3.4.2 Mass flow rate in rotor

The Reynolds number for flow of the fluid inside the rotor can thus be calculated by Equation (32) and varies up to a value of 16,000 for a rotation speed of 3000 rev min^{-1} with volumetric efficiency at unity.

$$\mathrm{Re}_{suc} = \frac{2\rho v_{suc}r_{pt,suc}}{\mu} = \frac{2\dot{m}_d}{\pi r_{pt,suc}\mu} \tag{32}$$

3.4.3 Convective heat transfer in shaft

The intake of fluid through the rotor first goes through the rotating shaft and is classified as an axial flow through a rotating duct. The rotation of the shaft affects the flow of the fluid; the rotating walls help reduce turbulence in the flow at the vicinity of the wall and thus heat transfer decreases with higher rotation speeds [20–22]. Seghir-Ouali et al. [22] provide the heat transfer correlations for axial flow inside a rotating cylinder duct with a constant heat flux in Equations (33) and (34).

$$\begin{aligned}&\mathrm{Nu} = 0.01963\mathrm{Re}_{suc}^{0.9285} + 8.5101 \times 10^{-6}\mathrm{Re}_{\omega}^{1.4513}\ ,\\ &\text{for } 0 < \mathrm{Re}_{suc} < 3 \times 10^4\ , 1600 < \mathrm{Re}_{\omega} \le 2.77 \times 10^5\end{aligned} \tag{33}$$

$$\mathrm{Nu} = 2.85 \times 10^{-4}\mathrm{Re}_{\omega}^{1.19}\ , \qquad \mathrm{Re}_{\omega} > 2.77 \times 10^5 \tag{34}$$

where Re_ω is the rotational Reynolds number given as follows:

$$\mathrm{Re}_{\omega} = \frac{2r_{pt}^2\omega_{shaft}\rho}{\mu} \tag{35}$$

3.4.4 Convective heat transfer in rotor

It is an internal laminar flow in the suction line inside the rotor with uniform wall temperature. The heat transfer coefficient is thus given in Equation (36).

$$\mathrm{Nu} = 3.66\ , \quad \mathrm{Re}_{suc} < 10^4 \tag{36}$$

3.5 Linear Algebra Equations for Component Elements

With 12 elements, there will be 12 simultaneous equation, the equations can be arranged into a matrix and solved as a linear algebra equation to obtain the temperatures.

As an example, for the cylinder element *c*1 shown in Figure 1(b), it is affected by free convection and heat transfer from element *c*2. Hence, the heat transfer to and from the element can be written as shown in Equation (37) which is rearranged into Equation (38).

$$H_{c1,c2}(T_{c1} - T_{c2}) + H_{c1,\infty}(T_{c1} - T_{\infty}) = 0 \tag{37}$$

$$\left(H_{c1,c2} + H_{c1\infty}\right)T_{c1} + H_{c1,c2}T_{c2} = H_{c1,\infty}T_{\infty} \tag{38}$$

where,

$$H_{c1,c2} = H_{c2,c1} = \frac{k_{steel}A_{c1,c2}}{l_{c1,c2}} = \frac{2k\pi r_{shaft}^2}{l_{c1} + l_{c2}} \tag{39}$$

$$\begin{aligned} H_{c1,\infty} &= \frac{k_{air}A_{c1,\infty}}{l_{c1,\infty}}\left(0.119\mathrm{Re}_r^{2/3}\right) + 0.25A_{c1,\infty}\sigma(T_{c1} + T_{\infty})(T_{c1}^2 + T_{\infty}^2) \\ &= \frac{2k_{air}\pi r_{shaft}l_{c1}}{l_{c1}}\left[0.119\left(\frac{2\rho\omega_{shaft}r_{shaft}^2}{\mu}\right)^{2/3}\right] \\ &\quad + 0.25\sigma(T_{c1} + T_{\infty})(T_{c1}^2 + T_{\infty}^2)\left(2\pi r_{shaft}l_{c1}\right) \end{aligned} \tag{40}$$

Due to the insulating PEEK bearing liners separating the cylinder from the housing shell, there is no coupling of temperatures between these two components. Furthermore, the rotor is also considered to be a separate system due to the insulating property of PEEK for heat conduction. Hence, each of the components will have their own separate matrices as shown in Equations (41) – (43). $\boldsymbol{T}$ represents the component element temperatures, $\boldsymbol{X}$ represents the heat transfer relations and $\boldsymbol{Y}$ represents the loss to surroundings and heat source terms.

$$\boldsymbol{X}_c\boldsymbol{T}_c = \boldsymbol{Y}_c \tag{41}$$

$$\boldsymbol{X}_r\boldsymbol{T}_r = \boldsymbol{Y}_r \tag{42}$$

$$\boldsymbol{X}_h\boldsymbol{T}_h = \boldsymbol{Y}_h \tag{43}$$

Equations (41) to (43) are then solved for their respective $\boldsymbol{T}$ matrices which contains all the elements' temperature values for each component using Gaussian Elimination. The solution would give the steady-state operating temperatures of the components for the RV compressor prototype.

3.6 Preliminary Analysis

The operating conditions are shown in Table 3. It is assumed that there is no internal leakage occurring between the working chambers.

Table 3: Operating Conditions and Ambient Temperature

Operating Speed, rev min^{-1}	1,000 / 2,000
Working Fluid	Air
Suction Pressure, bar (abs)	1.0
Suction Temperature, °C	27.0
Discharge Pressure, bar (abs)	2.0 / 5.0
Coefficient of Friction	0.4
Ambient Temperature, °C	27.0

The temperatures of the components at a discharge pressure of 2 bar (abs) are presented in Figure 6. The temperature of the upper PEEK bearing liner sleeve *s1* can be taken as the mean temperature of elements *c2* and *h1* which is 58.5°C. Similarly, the temperature of the lower PEEK bearing liner sleeve *s2* is taken

to be the mean temperature of elements *c4* and *h4* which is 72.4°C. For 5 bar (abs) discharge pressure in Figure 7, the respective temperatures of the upper and lower bearing sleeves are 120.5°C and 149.5°C, respectively.

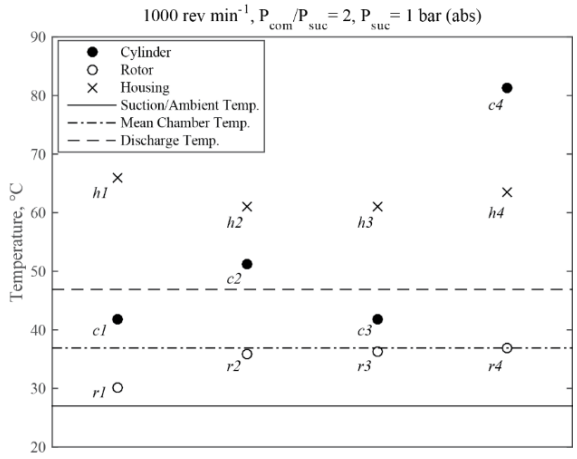

Figure 6: Predicted Steady-state Component Temperatures for 1 bar Pressure Difference

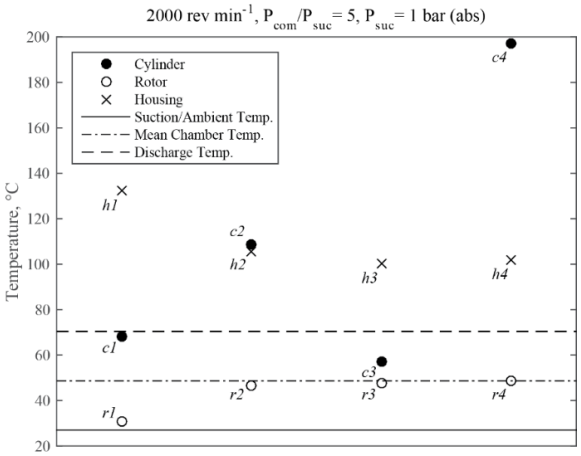

Figure 7: Predicted Steady-state Component Temperatures for 4 bar Pressure Difference

From the analysis, it is noted that the steady-state operating temperature of the rotor would be approximately the same as the average chamber temperature as the rotor has poor thermal conductivity. The rotor shaft (*r1*) would be at a lower temperature due to enhanced heat dissipation when the shaft rotates.

For the cylinder, there is a wide variation between the different elements. Friction heating at the shaft elements (*c2*, *c4*) result in higher temperatures while the rotation of the cylinder enhances heat dissipation in elements *c1* and *c3*. The very high temperature at shaft element *c4* is due to its large diameter in which there is more friction heat.

The housing shell is cooled by free convection on the external surfaces and by the discharge fluid on the inner surfaces. Thus, its temperature variation is not as significant.

The current analysis was conducted under ideal conditions with no internal leakage. Under practical operating conditions, the circulation of leakage fluid between the working chambers would no doubt cause the average chamber temperature and discharge temperature to rise, thus increasing the temperatures of the compressor. The trend would be akin to the increase in the element temperatures between Figure 6 and 7 in which Figure 7 shows a higher chamber temperature.

4. Conclusion

The thermal modelling of an oil-free compressor is presented using the lumped thermal conductance method and a preliminary analysis of the operating temperature was conducted, albeit assuming ideal conditions with no internal leakage. A summary of the analysis is as follows:

- The steady-state operating temperature of the rotor is close to that of the mean chamber temperature. On the other hand, the walls of the suction line in the rotor shaft are rotating, resulting in enhanced heat dissipation and thus, lower temperature values for the rotor shaft.
- The lower cylinder bearing has the highest temperature due to high friction loss caused by a large bearing diameter. On the other end, the continuous flow of working fluid into and out of the cylinder chamber helps to cool the overall component.
- Internal leakage under practical operating conditions would cause the chamber temperature to increase which consequentially increases the temperature of the components.
- Excessive friction heating at the shafts can be mitigated by redesigning the shafts to have smaller diameters and the use of ball/roller bearings instead of plain journal bearings

Nomenclature

A	Area (m^2)
F	Force (N)
$F_{i\rightarrow j}$	View factor (–)
h	Heat transfer coefficient ($W\ m^{-2}\ K^{-1}$)
k	Thermal conductivity ($W\ m^{-1}\ K^{-1}$)
l	Length (m)
Nu	Nusselt number (–)
Pr	Prandtl number (–)
Q	Heat (J)
R	Thermal resistance ($m^2\ K\ W^{-1}$)
Ra	Rayleigh number (–)
Re	Reynolds number (–)
r	Radius; radial distance (m)
T	Temperature (K)
v	Velocity ($m\ s^{-1}$)
ε	Emissivity (–)
σ	Stefan-boltzmann constant ($W\ m^{-2}\ K^{-4}$)
ω	Angular velocity ($rad\ s^{-1}$)

References

1. Todescat, M. L., Fagotti, F., Prata, A. T., & Ferreira, R. T. S. (1992). Thermal Energy Analysis in Reciprocating Hermetic Compressors. In International Compressor Engineering Conference.
2. Weber, G. C., Lajus, F., Ribas, F. A., & Fonseca, J. N. (2010). A Simplified Thermal Model for a CO2 Compressor. In International Compressor Engineering Conference.
3. Deschamps, M. J. O. and M. C. D. and C. J. (2015). Thermal modelling and analysis of an oil-free linear compressor. IOP Conference Series: Materials Science and Engineering, 90(1), 12016.
4. Ooi, K. T. (2003). Heat transfer study of a hermetic refrigeration compressor. *Applied Thermal Engineering*, *23*(15), 1931–1945.

5. Incropera, F. P., Bergman, T. L., DeWitt, D. P., Lavine, A. S., (2011). *Fundamentals of Heat and Mass Transfer* (6th ed.). Wiley.
6. Tan, K. M., & Ooi, K. T. (2011). Heat transfer in compression chamber of a revolving vane (RV) compressor. *Applied Thermal Engineering*, *31*(8–9), 1519–1526.
7. Liu, R., & Zhou, Z. (1984). Heat Transfer Between Gas and Cylinder Wall of Refrigerating Reciprocating Compressor. In International Compressor Engineering Conference.
8. Gardiner, S. R. ., & Sabersky, R. . (1978). Heat transfer in an annular gap. *International Journal of Heat and Mass Transfer*, *21*(12), 1459–1466.
9. Becker, K. M. (1963). Measurements of convective heat transfer from a horizontal cylinder rotating in a tank of water. *International Journal of Heat and Mass Transfer*, *6*(12), 1053–1062.
10. Özerdem, B. (2000). Measurement of convective heat transfer coefficient for a horizontal cylinder rotating in quiescent air. *International Communications in Heat and Mass Transfer*, *27*(3), 389–395.
11. Bardon, J. P. (1994). Bases physiques des conditions de contact thermique imparfait entre milieux en glissement relatif. *Revue générale de thermique*, *33*(386).
12. Chantrenne, P., & Raynaud, M. (1997). A microscopic thermal model for dry sliding contact. *Int. J. Heat Mass Tran.*, *40*(5), 1083–1094.
13. Cengel, Y. A., & Boles, M. A. (2006). *Thermodynamics: An Engineering Approach* (5th ed.). McGraw Hill.
14. Chantrenne, P., & Raynaud, M. (2001). Study of a macroscopic sliding contact thermal model from microscopic models. *International Journal of Thermal Sciences*, *40*(7), 603–621.
15. EFunda. (n.d.). eFunda: Properties of Alloy Steel AISI 4140. Retrieved July 23, 2014, from http://www.efunda.com/Materials/alloys/alloy_steels/show_alloy.cfm?ID=AISI_4140&prop=all&Page_Title=AISI 4140
16. McAdams, W. H. (1954). *Heat Transmission* (3rd Ed.). New York: McGraw-Hill.
17. Churchill, S. W., & Chu, H. H. S. (1975). Correlating equations for laminar and turbulent free convection from a vertical plate. *International Journal of Heat and Mass Transfer*, *18*(11), 1323–1329.
18. Cobb, E. C., & Saunders, O. A. (1956). Heat Transfer from a Rotating Disk. *Proceedings of the Royal Society of London. Series A, Mathematical and Physical Sciences*, *236*(1206), 343–351.
19. Wagner, C. (1948). Heat Transfer from a Rotating Disk to Ambient Air. *Journal of Applied Physics*, *19*(9).
20. Reich, G., Weigand, B., & Beer, H. (1989). Fluid flow and heat transfer in an axially rotating pipe -I. Effect of rotation on turbulent pipe flow. *International journal for Heat and Mass transfer*, *32*(9), 551–562.
21. Reich, G., Weigand, B., & Beer, H. (1989). Fluid flow and heat transfer in an axially rotating pipe -II. Effect of rotation on laminar pipe flow. *International journal for Heat and Mass transfer*, *32*(9), 563–574.
22. Seghir-Ouali, S., Saury, D., Harmand, S., Phillipart, O., & Laloy, D. (2006). Convective heat transfer inside a rotating cylinder with an axial air flow. *International Journal of Thermal Sciences*, *45*(12), 1166–1178.